Available online at www.sciencedirect.com
ScienceDirect
Deep-Sea Research I 55 (2008) 108–127
DEEP-SEA RESEARCH PART I
www.elsevier.com/locate/dsri

A bottom-up view of the biological pump: Modeling source funnels above ocean sediment traps

D.A. Siegel[a,*], E. Fields[a], K.O. Buesseler[b,1]

[a]*Department of Geography, Institute for Computational Earth System Science, University of California, Santa Barbara, CA 93106-3060, USA*

[b]*Department of Marine Chemistry and Geochemistry, Woods Hole Oceanographic Institution, Woods Hole, MA 02543, USA*

Received 5 July 2006; received in revised form 22 October 2007; accepted 28 October 2007
Available online 6 November 2007

Abstract

The sinking of particles that make up the biological pump is not vertical but nearly horizontal. This means that the locations where the particles are formed may be distant from their collection in a sediment trap. This has led to the development of the concept of the statistical funnel to describe the spatial–temporal sampling characteristics of a sediment trap. Statistical funnels can be used to quantify the source region in the upper ocean where collected particles were created (source funnels) or the location of the collected particles during that deployment (collection funnels). Here, we characterize statistical funnels for neutrally buoyant, surface-tethered and deep-ocean moored trap deployments conducted just north of Hawaii in the Pacific Ocean. Three-dimensional realizations of the synoptic velocity field, created using satellite altimeter and shipboard acoustic Doppler current profiler data, are used to advect sinking particles back to their source for sinking velocities of 50–200 m per day. Estimated source- and collection-funnel characteristics for the 5-day collections made by neutrally buoyant and surface-tethered traps are similar with typical scales of several km to several 10s of km. Deep-moored traps have daily source-funnel locations that can be many 100s of km distant from the trap and have long-term containment radii that range from 140 to 340 km depending upon sinking rate. We assess the importance of particle source regions using satellite estimates of chlorophyll concentration as a surrogate for the spatial distribution of particle export. Our analysis points to the need to diagnose water-parcel trajectories and particle sinking rates in the interpretation of sinking-particle fluxes from moored or freely drifting sediment traps, especially for regions where there are significant horizontal gradients in the export flux.

> But whence come the little siliceous and calcareous shells…[brought up] from the depth of over miles? Did they live in the surface waters immediately above? Or is their habitat in some remote part of the sea, whence, at their death, the currents were set forth as pallbearers, with the command to deposit the dead corpses where the plummet found them? (Maury, 1858).

Keywords: Sinking-particle flux; Carbon export; Eddies; Advection; Collection funnels

*Corresponding author. Tel.: +1 805 893 4547; fax: +1 805 893 2578.
E-mail addresses: davey@icess.ucsb.edu (D.A. Siegel), fields@icess.ucsb.edu (E. Fields), kbuesseler@whoi.edu (K.O. Buesseler).
[1]Tel.: +1 508 289 2309; fax: +1 508 457 2193.

0967-0637/$ - see front matter © 2007 Elsevier Ltd. All rights reserved.
doi:10.1016/j.dsr.2007.10.006

1. Introduction

Knowledge of the controls on the export flux of organic carbon from the euphotic zone to depths of the mesopelagic, the so-called twilight zone, is needed in order to predict the magnitude of the biological pump and its changes over time (e.g., Fasham, 2003; Buesseler et al., 2007a). This knowledge can be gained only by understanding the production of sinking particulate matter within the euphotic and its remineralization as it sinks to depth. Hence, there is a compelling need to sample sinking particles, their flux as a function of depth and the rates at which they are produced in the euphotic zone. Experiments to assess the production of sinking particles and their vertical flux were one of the focused objectives of the major biogeochemical research programs of the past decade (e.g., Asper et al., 1992; Michaels and Knap, 1996; Karl et al., 1996; Christian et al., 1997; Martin et al., 1987). These experiments nearly always resulted in a poor correspondence between determinations of primary production rates measured in the euphotic zone and the sinking flux at depth.

This raises the question why are the observations between primary production and export flux often poorly related? Is the problem in the accuracy with which sinking flux or primary production measurements are made? Or is it something about particle export itself? For example, is there an intrinsic time lag or nonlinear response in the relationship between primary production and export flux? Or is it simply a mismatch of the sampling time and space scales between these two factors?

Present methods for collecting sinking material rely primarily on the deployment of sediment traps, which, in principle, collect the sinking-particle flux similar to snow or rain gauges. However, the slow sinking rates of marine particles (typically 200 m/day and less) make these measurements difficult to make and nearly impossible to validate and standardize (Buesseler, 1992, 1998; Buesseler et al., 1994, 2007b; Asper, 1996; Gardner, 2000). This is made more difficult by the degree to which hydrodynamic processes affect the collection of particles (e.g., Gust et al., 1994), by faunal interactions (i.e., swimmers) with the collected materials (e.g., Karl and Knauer, 1989; Michaels et al., 1990; Gardner, 2000) and by the degradation of organic matter within the trap (Gardner, 2000). The known difficulties in quantitative particle trapping have created a plethora of proposed solutions from neutrally buoyant traps, which minimize the hydrodynamic effects (e.g., Asper, 1996; Valdes and Price, 2000; Buesseler et al., 2000; Lampitt et al., 2004), to screens that attempt to reduce swimmers in the traps (e.g., Karl and Knauer, 1989) to mechanical swimmer avoidance devices (e.g., Coale, 1990; Peterson et al., 1993; Hansell and Newton, 1994).

The slow sinking rate of marine particles also raises the question of the source of particles collected by traps. Did they come from directly above the trap or, as Maury (1858) suggested, were they advected over great distances as they sink? A particle sinking at 100 m per day through a horizontal current of 5 cm/s will sink with a trajectory that is only 1.3° below the horizontal horizon. Simply, the sinking-particle flux is nearly horizontal. This particle will take 5 days to sink to a sediment trap deployed at 500 m and 50 days to be collected by a trap moored at 5000 m. During this time, the same particle will have traveled 22 km to the shallow trap and 220 km to the deep trap.

Horizontal currents are variable on time and space scales ranging from seconds to years and from meters to 1000s of km. This variability will act to disperse the paths of particles horizontally as they sink through the water column. This realization forced researchers to develop the concept of a statistical funnel that contains the origin of particles that are collected by sediment traps (Deuser et al., 1990; Siegel et al., 1990; Siegel and Deuser, 1997; Waniek et al., 2000, 2005). A statistical funnel describes how a sediment trap samples the sinking rain of particles above it. If, for example, the spatial distribution of export is uniform, then the details of where a sediment trap samples sinking particles are unimportant. However, if the export flux has significant spatial gradients, then the trap may not be sampling the export from directly above it (e.g., Siegel et al., 1990). This can lead to instances where the sinking-particle flux may increase with depth or show vertical patterns that are unrelated to the actual processes of remineralization and particle aggregation and disaggregation actually acting on the sinking flux. Biogeochemical parameters are well known to have extensive spatial gradients on meso- and submeso-length and time scales—even in the open ocean (e.g., McGillicuddy et al., 1998; Wilson, 2003). Hence, it is critical to learn more about how sediment traps sample the rain of particles.

Here, we quantify statistical funnels for three deployment strategies used to measure the sinking flux of particles in the sea: surface-tethered

upper-ocean sediment traps, neutrally buoyant sediment traps (NBSTs) and deep-sea moored traps. Statistical funnels can be used to quantify the source region in the euphotic zone where particles were created (source funnels) or simply the location of the particles that were collected by the trap (collection funnels). Both have utility in the interpretation of experimental results. Here, we characterize source and collection funnels for three types of ocean sediment traps using data collected from the VERtical Transport In the Global Ocean (VERTIGO) cruise aboard the R/V *Kilo Moana* to Station ALOHA in the subtropical Pacific Ocean (June 22–July 9, 2004; Buesseler et al., 2007a). We show that trap type, deployment depth and particle sinking rate all contribute to trap sampling characteristics. We assess the importance of particle source funnels using satellite-determined chlorophyll concentrations as a surrogate for particle export and provide guidance future export-flux experiments.

2. Modeling statistical funnels

An analytical framework for determining statistical funnels above a sediment trap was introduced by Siegel et al. (1990) and Siegel and Deuser (1997) and is extended here to include traps that move in time and particles that can change their sinking rate. The theory follows the ith particle in time which is collected in the jth sediment trap, $\vec{x}_i(\vec{a}_j(T_i), t)$, which can be expressed as

$$\vec{x}_i(\vec{a}_j(T_i), t) = \vec{x}_i(\vec{a}_j(T_i), 0) + \int_0^t \vec{v}_i(\vec{x}(\vec{a}_j(T_i), t'))\,\mathrm{d}t', \tag{1}$$

where $t = 0$ is the time that the ith sinking particle has sunk from the location of its formation, T_i is the time the ith particle is collected by the trap at location, $\vec{a}_j(T_i)$, and $\vec{v}_i(\vec{x}_j(\vec{a}_j(T_i), t))$ is the velocity (fluid and sinking) acting on the particle through its trajectory. The particle and the trap intersect at the time of the particle's collection, T_i, or $\vec{x}(\vec{a}_j(T_i), T_i) = \vec{a}_j(T_i)$. Hence, collected particle locations can be quantified knowing $\vec{v}_i(\vec{x}_j(\vec{a}_j(T_i), t))$ and $\vec{a}_j(T_i)$.

The velocity acting on the sinking particle is the combination of fluid motions from ocean currents and the sinking rate of the particle, or

$$\vec{v}_i(\vec{x}_i(\vec{a}_j(T_i), t)) = \vec{u}(\vec{x}_i(\vec{a}_j(T_i), t)) + S_i(\vec{x}_i(\vec{a}_j(T_i), t))\hat{k}, \tag{2}$$

where $\vec{u}(\vec{x}_i(\vec{a}_j(T_i), t))$ is the fluid velocity field sampled at the location of the ith sinking particle, $S_i(\vec{x}_i(\vec{a}_j(T_i), t))$ is its sinking rate and $\hat{k}$ is the unit vector in the vertical (up) direction. This formulation allows the possibility that the sinking rate can vary as a function of depth because of changes in particle composition or digenetic state (e.g., Berelson, 2002; Armstrong et al., 2002). The effects of vertical fluid motions are not considered as these velocities are rarely greater than a meter per day, which is much smaller than typical particle sinking speeds. The collection time is related to the sinking rate as

$$\int_0^{T_i} S_i(\vec{x}_i(\vec{a}_j(T_i), t'))\,\mathrm{d}t' = \hat{k} \cdot \vec{a}_j(T_i) = H_j, \tag{3}$$

where H_j is the depth of the jth sediment trap. If the sinking rate is independent of depth, Eq. (3) reduces to $T_i = H_j/S_i$, where S_i is the mean sinking rate of the ith particle.

The design of the sediment trap will have a bearing on the scales of circulation that contribute to a trap's collection. Moored traps are fixed to the sea floor, and all scales of motion advect particles relative to the trap. Drifting traps are embedded in the flow and are advected along with the sinking particles. This means that drifting traps will filter some of the larger scales of motion whereas deep-moored traps will sample the effects of all scales of motion. The type of drifting trap may also be important. Surface-tethered trap arrays vertically integrate horizontal motions in some way, while neutrally buoyant traps move with the currents at the depth of their deployment. Differences between the sampling characteristics between a neutrally buoyant trap and a surface-tethered trap are likely related to the scales of motion of the vertical shear of the currents above the trap and the drag characteristics of the tethered trap array.

Determination of funnel characteristics is straightforward given the three-dimensional, time-dependent velocity field, the time course for the particle sinking rate and the trajectory in space and time of the sediment trap (Eqs. (1)–(3)). The key step is separating the flow into a local time-mean and time-varying components (see below). The local mean velocity field is used to estimate the center of mass of a cloud of sinking particles and dispersion about this deterministic location is calculated using only the time-varying components of motion to assess the size of the collection funnel at a given time (Siegel and Deuser, 1997). This time decomposition

is similar in approach to the puff-particle modeling turbulent dispersion where the location of particle clouds is determined by the large-scale velocity field, and the sizes of the clouds grow because of small-scale mixing processes (e.g., de Haan and Rotach, 1998). Knowing the three-dimensional velocity field and its partitioning in time, sinking-particle trajectories are integrated backward in time from the collection time to the origin at time equal to zero (when the particle reaches the euphotic zone or upper-ocean mixed layer) or over the time period when particles are collected during the trap's deployment (which may be shorter than the total sinking time for a particle leaving the upper ocean). By ensemble averaging over many trajectories we get a depiction of the statistical funnel for each collection and sinking rate that takes into account the large space, long time scales of the flow field.

There are two depictions of the statistical funnel concept: the *source funnel*, which describes where in the euphotic zone exported particles are formed, and the *collection funnel*, which quantifies where the particles collected during a trap's deployment were in the water column. This difference is simply due to the fact that not all (and often none) of the particles collected by a trap will have exited the upper layers of the ocean during the time the trap is deployed. For upper-ocean traps, particle sinking times are of the same order of magnitude as trap deployment times. These subtleties may be important. A researcher interested in connecting the collected particles to local water-column processes would want to sample the trap's collection funnel. On the other hand, if one wanted to relate flux determinations with upper-ocean primary production, one would need to quantify the trap's source funnel.

3. Observations of the horizontal velocity field

The horizontal velocity field and its change over time are observed using a variety of tools, including satellite altimeter estimates of absolute geostrophic currents, shipboard acoustic Doppler current profiler (ADCP) determinations (Firing, 1996) and satellite-tracked surface drifters. Satellite altimetry determinations of absolute dynamic topography are used to provide a large-scale view of the geostrophic flow field (Fig. 1). Merged absolute dynamic topography fields from Ssalto/Duacs (www.aviso.oceanobs.com/html/donnees/duacs/welcome_uk.html) were used. These data are objectively analyzed dynamic topography fields on a $\frac{1}{3}^{\circ}$ resolution grid with a temporal resolution of 3.5 days where observations from as many as six satellites are merged together for the period 2001–2004. Real-time altimetry observations (Leben et al., 2002) were analyzed at sea for cruise planning.

The time evolutions of absolute dynamic topography and horizontal currents spanning the VERTIGO experiment are shown for every 2 weeks in Fig. 1. Station ALOHA (the location of the crosshairs in Fig. 1) was within an anti-cyclonic eddy feature (clockwise circulation) with a diameter of ~150 km. The cyclone propagated slowly westward during the experiment, which resulted in lower advective velocities for the first trap deployment period than the second. Typical mesoscale velocities at the surface were several 10s of km per day.

The R/V *Kilo Moana* deployed an RD Instruments (San Diego, CA) ocean observer 38 kHz ADCP system, which provided profiles of horizontal current every 15 min with depth starting at 50 m in bins of 20 m. Broadband and narrowband pings were interleaved and used for obtaining currents over the upper 550 m, while the deeper narrowband pings were used to obtain currents to 1200 m. For modeling the deep-trap sampling characteristics, an annual mean sub-inertial speed profile was created using available ADCP data from all cruises to Station ALOHA for 2004. Below 1200 m, a constant value for the root-mean-square (RMS) currents was assumed (see below).

Horizontal currents from the ADCP system are partitioned into sub-inertial and currents with frequencies greater than the local inertial period (31 h; Fig. 2). Diurnal, semi-diurnal and inertial motions were removed by performing a harmonic analysis on 3-day intervals, generating a daily set of tidal coefficients (following Firing, 1996). The RMS amplitude for each of the three harmonic components is shown in the left panel of Fig. 2. Energy levels are greater for the inertial frequency band compared with the diurnal and semi-diurnal tidal frequencies. RMS amplitudes of these high-frequency motions decrease from as much as 4 km/day near the sea surface to about 1 km/day at 500-m depth.

The residual, sub-inertial currents are objectively analyzed after removing the high-frequency components to produce time-dependent, three-dimensional fields of horizontal currents (e.g., Bretherton et al., 1976; Daley, 1994; Siegel et al., 1999). The velocity covariance function is modeled from the satellite altimetry observations and is assumed to be

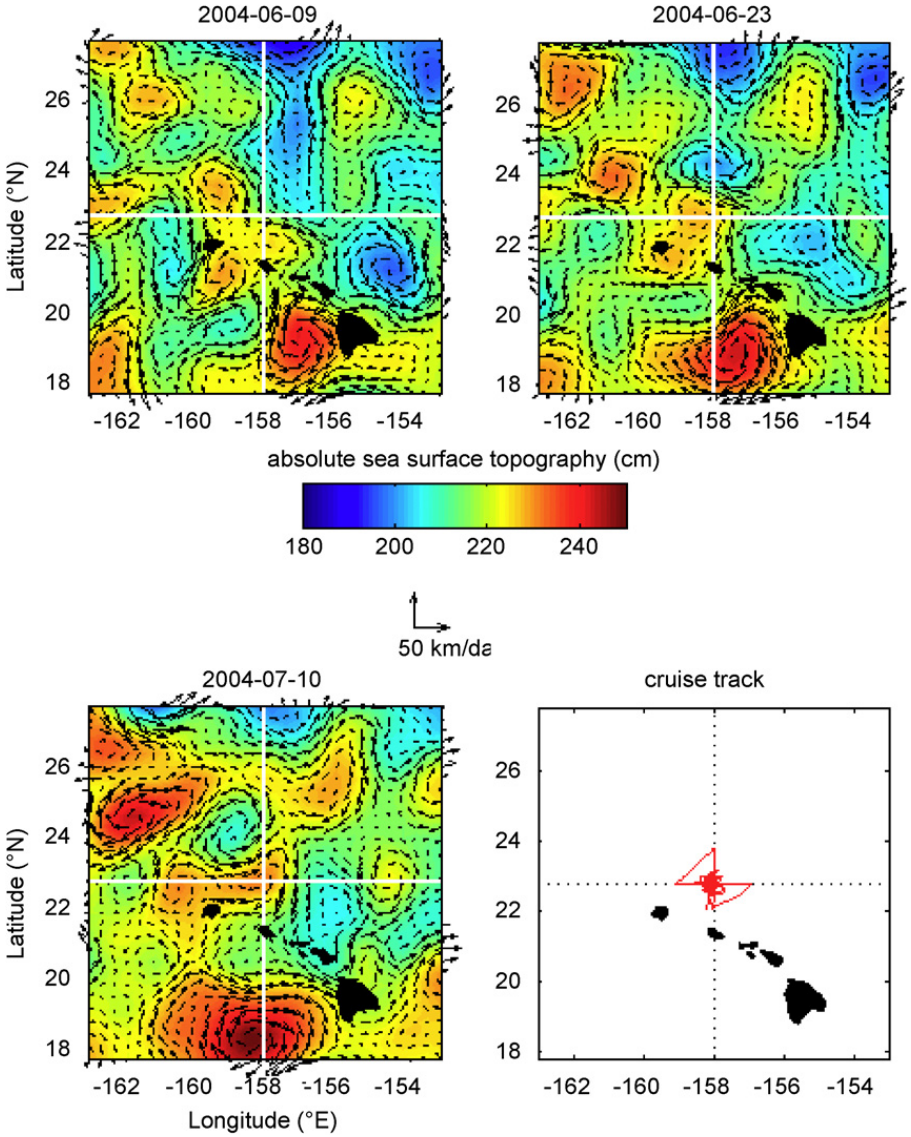

Fig. 1. Absolute sea surface topography (cm) with geostrophic current vectors (in km/day) for the time period surrounding the VERTIGO-ALOHA field program. High absolute sea level is red while blue are low sea levels. Station ALOHA is centered where the white lines cross. The lower-right panel shows the cruise track for the VERTIGO-ALOHA field program.

horizontally isotropic. Mean sub-inertial currents at depths of 50, 150, 310 and 510 m are shown in Fig. 3 for June 27, 2004. The objectively analyzed currents show the clockwise circulation of the anti-cyclone observed from satellite altimetry (Fig. 1). For this analysis date, Station ALOHA is nearly in the center of this eddy. The anti-cyclonic signature is apparent for the upper three level surfaces shown (50, 150 and 310 m), though its magnitude is much reduced at 310 m and is absent at 510 m. The mean sub-inertial velocity profile over the entire experiment from the central site (Station ALOHA) is shown in the right panel of Fig. 2. The meridional component is only a couple of km per day, while the zonal velocity is large in the upper 250 m, with a maximum eastward velocity of nearly 12 km per day at 110 m depth. Time evolution of objectively mapped currents at 50 m for dates June 20 and 27 and July 4 and 11, 2004 is shown in Fig. 4. The circulation is predominately anti-cyclonic though the location and strength of the mesoscale feature change over time. In particular, the sub-inertial current fields are especially large for the last half of the experiment (Fig. 4). The sub-inertial currents, along with the modeled high-frequency motions, are used to predict particle origins for the upper-ocean sediment traps.

The difference between the observed ADCP currents and the sum of the objectively analyzed sub-inertial currents and the modeled high-frequency

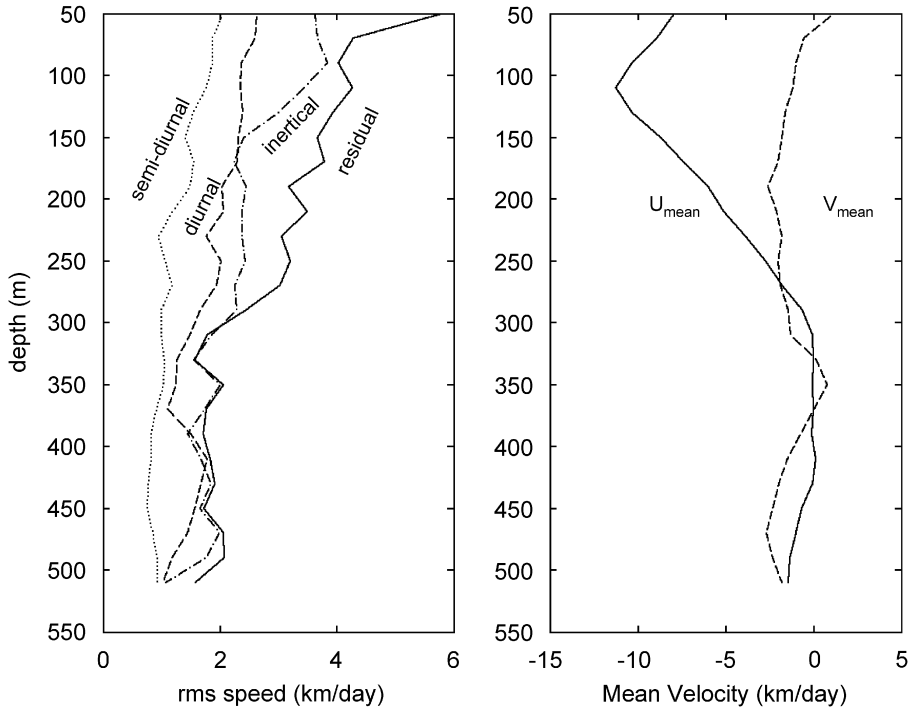

Fig. 2. Current partitioning evaluated from the ADCP system during the VERTIGO-ALOHA field program. In the left panel, the root-mean-square (RMS) velocity profiles are shown for the semi-diurnal (dotted line; 12.4 h) and diurnal (dashed line; 24 h) tidal components and the inertial (dashed-dotted line; 31 h) periods as well as the residual current RMS profile (solid line; defined as the difference between the objectively mapped sub-inertial currents and the measured sub-inertial currents). Fitting of the super-inertial currents is described in the text. In the right panel, the mean vertical profiles from the objectively mapped sub-inertial currents at Station ALOHA during the VERTIGO-ALOHA field program (the solid line is to the east and dashed is to the north) are shown.

motions defines the unresolved or residual currents. The RMS amplitudes of the residual currents are somewhat larger than the amplitudes of the high-frequency components within the upper 200 m and this difference decreases with depth (Fig. 2). The RMS amplitudes of the residual currents are considerably smaller than those found for the objectively mapped sub-inertial currents (Fig. 3) as well as the weak mean current (Fig. 2). The residual currents are used to estimate the extent of individual funnels about the deterministic paths calculated using the analyzed currents.

4. Sediment-trap deployments

Three types of ocean sediment traps were deployed during VERTIGO: drifting traps at a single depth tethered to a buoy at the sea surface, near-surface isobaric following traps and fixed traps moored to the bottom (Buesseler et al., 2007a). The first were surface-tethered drifting traps with collection tubes deployed at depths of 150, 300 and 500 m. They are referred to as "clap" traps as the collection tubes are programmed to close at the end of the sampling interval. The clap traps are drouged with a "holey sock" drogue located 3–5 m below the trap in an attempt to reduce local hydrodynamic velocities. Trap array location was transmitted to the ship in real time.

The second type of traps were the NBSTs (Valdes and Price, 2000; Buesseler et al., 2000, 2007a; Stanley et al., 2004). These traps are designed to sink to a preprogrammed depth, collect sinking particles while being advected by local currents, close at depth and then float back to the surface after their 3- to 5-day mission is completed. By moving with their local water mass, the NBSTs are designed to minimize hydrodynamic effects. However, their location in space is not known until the mission has completed and they have risen to the surface and contacted the ship. Real-time estimates of final trap location were made at sea which reduced search and recovery times. A total of 14 NBST deployments were successfully made for nominal depths of 150, 300 and 500 m.

Last, a bottom-moored sediment-trap array has been deployed at the HOT site since 1992 (e.g., Karl et al., 1996). The ALOHA-XI mooring was deployed in November 2003 (22°50.5′N, 157°52.4′W in 4800-m depth). This array consists of two Parflux

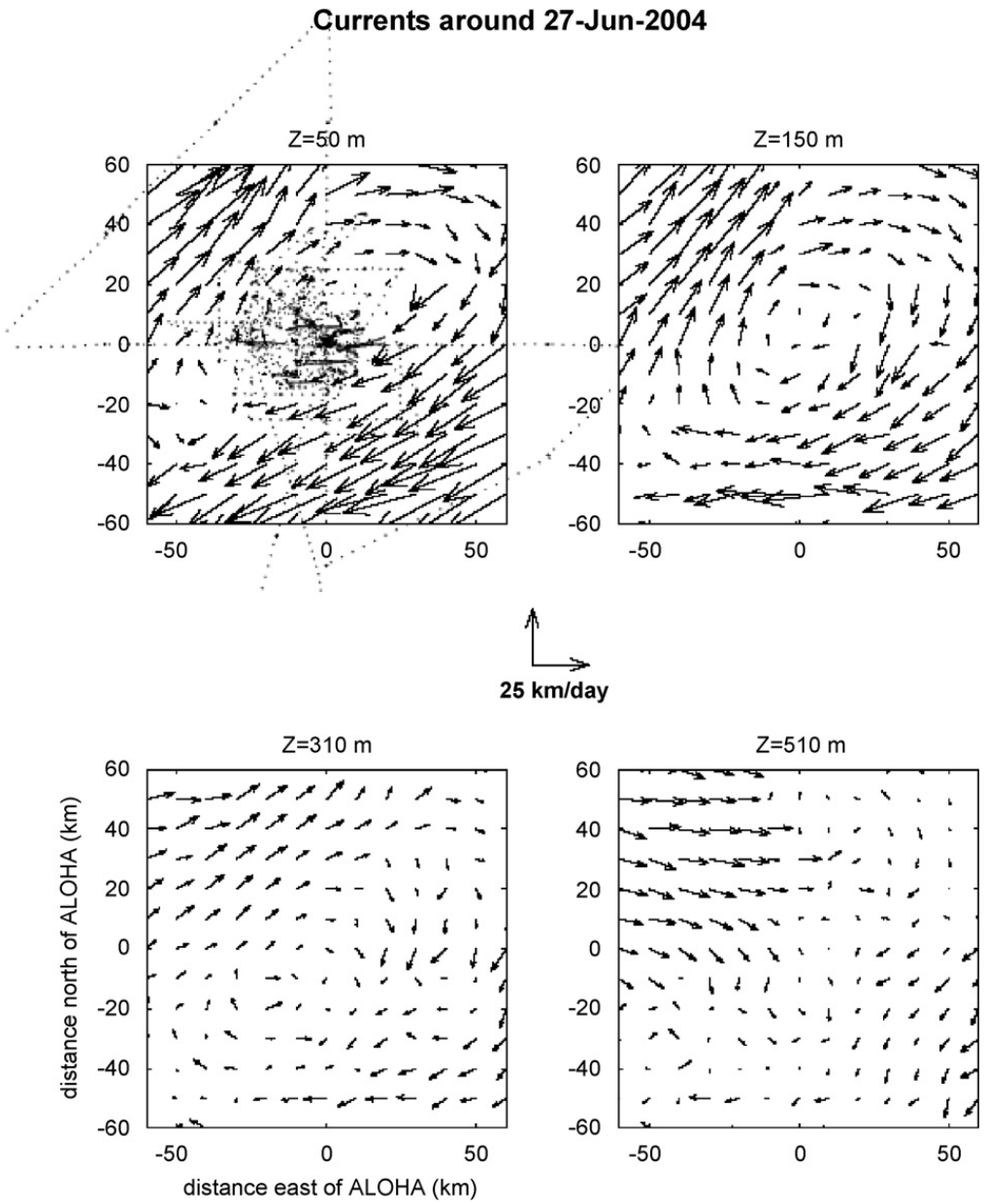

Fig. 3. Horizontal current vectors at depths of 50, 150, 310 and 510 m (from upper left to lower right) from the VERTIGO-ALOHA field program for June 27, 2004. The ship track is shown in the upper-left panel. Currents are objectively mapped assuming that the flow field is horizontally non-divergent (see text for details).

MK7-21 sequencing sediment collectors located at depths of 2800 and 4000 m. A separate sampling cup is rotated into the collector position on a 15- to 20-day cycle. Calculations of source-funnel characteristics are made for the 4000-m trap.

Details of the surface-tethered and NBST deployments and drift characteristics are given in Table 1. Locations for the clap traps are from position records, whereas NBST locations are calculated using the current data. Differences between the calculated and actual recovery locations were typically less than 5 km. Deployment times ranged from 3 to 5 days, allowing longer collection times for the deeper traps. Trap drift distances can be measured end to end (deployment location to recovery location) or following the trap as it drifts, the path distance. Typical values of end-to-end distances were 5–30 km with speeds ranging from 1 to more than 10 km per day. Path distances ranged from 20 to ~50 km corresponding to along-path speeds of 4–15 km per day. Both measures of drift speed were greater for the second deployment than the first. Trap drift speeds were generally similar for both the NBST and clap trap deployments (Table 1).

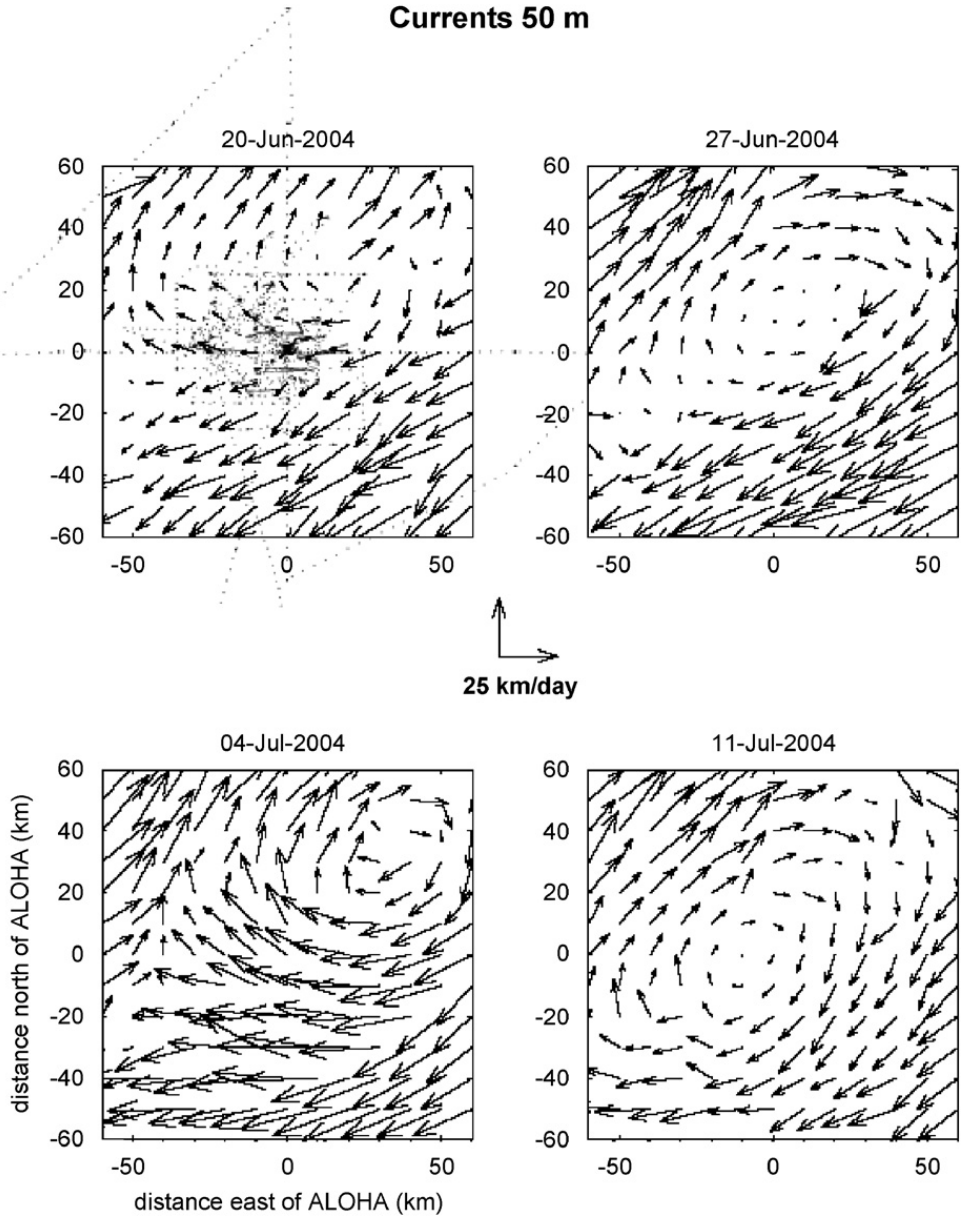

Fig. 4. Time varying mean horizontal current analyses for 50 m during the VERTIGO-ALOHA field program. The ship track is shown in the upper-left panel. Currents are objectively mapped assuming that the flow field is horizontally non-divergent (see text for details).

5. Source and collection funnels for upper-ocean sediment traps

An example of both source and collection funnels for particles sinking into a neutrally buoyant trap is shown in Fig. 5. Particles are modeled sinking into a 500-m NBST during the second deployment period at a rate of 50 m/day. The solid circles represent collection funnels (where the collected particles in the trap came from within the water column), whereas the open circles represent the source funnels (where the particles originated from the upper ocean). The color of the funnels represents the time during deployment when the particles were collected. Several features of source and collection funnels are apparent. First, typical source funnels are <20 km distant from mean trap locations and, as expected, the collection funnels stretch from the trap toward the source funnels. Second, for a sinking rate of 50 m/day, none of the collected particles has actually come from the euphotic zone during the 5 days the trap is deployed and the mean depth from which collected particles have come is 373 m (Table 2). For this case, collection and source funnels are distinct from each other. Third, radii of the individual collection funnels, the size of each

Table 1
VERTIGO-ALOHA trap deployments and drift characteristics

Trap ID	Depth (m)	Deployment no.	Deployment times (day)	End-to-end distance (km)	Path distance (km)	End-to-end speed (km/day)	Path speed (km/day)
NB13	150	1	2.8	16.6	28.3	5.9	10.1
NB14	300	1	3.7	8.5	20.1	2.3	5.4
NB11	500	1	4.5	4.3	25.1	1.0	5.6
Clap	150	1	2.9	10.9	21.1	3.8	7.3
Clap	300	1	4.1	9.3	17.9	2.3	4.4
Clap	500	1	5.0	14.6	24.6	2.9	4.9
NB13	150	2	3.2	34.5	39.3	10.8	12.3
NB14	300	2	4.1	7.5	23.3	1.8	5.7
NB11	500	2	5.0	17.2	27.1	3.4	5.4
Clap	150	2	3.2	30.4	47.8	9.5	14.9
Clap	300	2	4.2	22.6	38.9	5.4	9.3
Clap	500	2	5.0	26.2	31.7	5.2	6.3

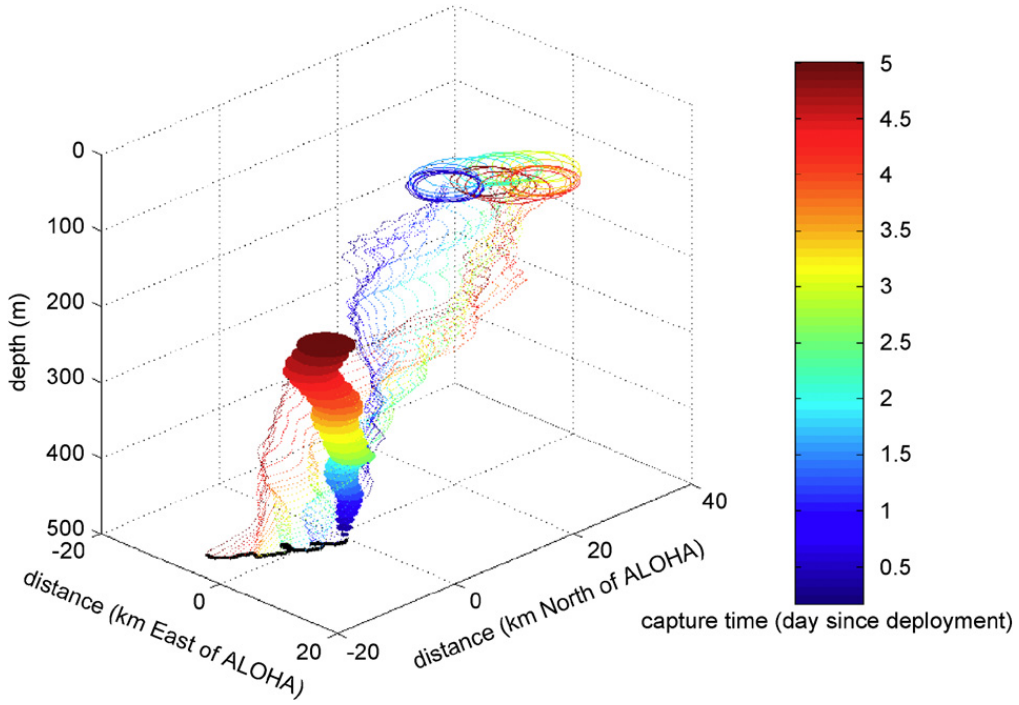

Fig. 5. Three-dimensional depiction of the collection (solid) and source (open) funnels for the second deployment of the 500-m NBST trap during VERTIGO-ALOHA. The color of the funnel depicts the collection time along the deployment time line. In these calculations, a sinking speed of 50 m/day is used. The deployment location is at the origin.

circle in Fig. 5, are smaller closer to the trap. The individual collection funnels, which are modeled using the RMS residual current profile (Fig. 2), grow due to the longer integration times of the earlier part of the trap's collection. Last, typical source-funnel locations are displaced <25 km from the trap's mean geographic location (Table 2).

An illustration of the role of particle sinking rate on the character of source and collection funnels is shown in Fig. 6 for the NBST deployed at 500 m during its second deployment (the two-dimensional representation of the 50-m/day case shown in Fig. 5 is the far right panel of Fig. 6). Collection and origin funnels overlap only for the most rapidly sinking particles during the last stages of the trap deployment (these coinciding collection funnels are represented by solid circles in Fig. 6). A complete lack of correspondence is seen for the 50-m/day sinking particles where the short collection time, slow particle sinking rate, slow currents at depth and a drifting trap all combine to place the collection funnels directly above the trap's recovery point.

Table 2
Funnel sampling characteristics during VERTIGO-ALOHA

Trap ID	Depth (m)	Deployment #	$\bar{S}$ (m/day)	Collect				Source at 50 m				
				$\bar{Z}_c$ (m)	$\bar{r}_c$ (km)	r'_c (km)	r^f_c (km)	$\bar{r}_s$ (km)	r'_s (km)	r^f_s (km)	$\Delta\bar{r}_s/\Delta t$ (km/day)	$\Delta\bar{r}'_s/\Delta t$ (km/day)
NB13	150	1	50	84	9.8	2.4	1.1	14.8	6.6	1.4	5.3	2.4
NB13	150	1	100	69	5.7	4.8	0.6	6.6	5.9	0.7	2.4	2.1
NB13	150	1	200	64	3.0	5.5	0.3	3.1	5.7	0.4	1.1	2.0
NB14	300	1	50	206	6.7	5.2	1.8	15.8	5.3	2.8	4.3	1.4
NB14	300	1	100	134	7.8	4.5	1.2	11.0	2.4	1.5	3.0	0.6
NB14	300	1	200	95	5.5	3.6	0.7	6.2	3.3	0.8	1.7	0.9
NB11	500	1	50	385	2.1	2.8	2.3	6.1	10.5	4.2	1.4	2.3
NB11	500	1	100	271	2.2	4.0	1.8	7.7	3.8	2.3	1.7	0.8
NB11	500	1	200	163	3.1	3.9	1.1	5.0	3.4	1.3	1.1	0.8
Clap	150	1	50	83	5.2	4.1	1.1	9.6	5.2	1.4	3.3	1.8
Clap	150	1	100	68	3.4	3.8	0.6	4.5	4.0	0.7	1.6	1.4
Clap	150	1	200	64	1.8	3.7	0.4	2.1	3.9	0.4	0.7	1.3
Clap	300	1	50	194	3.2	2.9	1.9	19.4	4.3	2.8	4.7	1.0
Clap	300	1	100	124	4.7	3.1	1.3	8.7	4.4	1.5	2.1	1.1
Clap	300	1	200	91	2.8	3.0	0.7	3.6	3.9	0.8	0.9	1.0
Clap	500	1	50	373	2.0	6.6	2.3	13.0	5.3	4.2	2.6	1.1
Clap	500	1	100	249	2.2	5.2	1.8	5.8	6.9	2.3	1.2	1.4
Clap	500	1	200	152	2.5	4.5	1.1	3.3	5.7	1.3	0.7	1.1
NB13	150	2	50	81	20.7	5.6	1.1	27.2	10.3	1.3	8.5	3.2
NB13	150	2	100	67	11.4	11.1	0.7	13.0	12.9	0.7	4.1	4.0
NB13	150	2	200	64	5.8	11.7	0.4	6.2	12.3	0.4	1.9	3.8
NB14	300	2	50	194	14.8	9.6	1.9	35.5	9.0	2.8	8.7	2.2
NB14	300	2	100	124	17.9	10.5	1.3	25.7	6.1	1.5	6.3	1.5
NB14	300	2	200	91	10.4	4.8	0.7	12.6	5.0	0.8	3.1	1.2
NB11	500	2	50	373	7.6	2.4	2.4	27.3	5.2	4.2	5.5	1.0
NB11	500	2	100	249	13.0	9.6	1.8	26.1	8.4	2.3	5.2	1.7
NB11	500	2	200	152	10.6	7.6	1.1	15.2	8.1	1.3	3.0	1.6
Clap	150	2	50	81	11.3	7.8	1.1	17.1	12.6	1.3	5.3	3.9
Clap	150	2	100	67	6.6	10.8	0.6	8.0	12.5	0.7	2.5	3.9
Clap	150	2	200	64	3.4	11.1	0.3	3.8	11.9	0.4	1.2	3.7
Clap	300	2	50	194	9.5	4.3	1.9	22.8	4.4	2.8	5.4	1.0
Clap	300	2	100	124	11.3	5.6	1.3	17.4	8.3	1.5	4.1	2.0
Clap	300	2	200	91	6.4	7.8	0.7	8.1	9.5	0.8	1.9	2.3
Clap	500	2	50	373	2.1	8.1	2.4	17.4	10.1	4.2	3.5	2.0
Clap	500	2	100	249	5.0	5.8	1.8	14.9	6.5	2.3	3.0	1.3
Clap	500	2	200	152	5.4	6.7	1.1	9.4	10.3	1.3	1.9	2.1

Note: $\bar{Z}_c$ is the mean depth of the collected particles during the trap deployment, $\bar{r}_c$ and $\bar{r}_s$ are the mean distance between the trap's location and the calculated collection and source funnels, r'_c and r'_s are estimates of spatial extent or patch scale of the individual collection and source funnels and r^f_c and r^f_s are the size of the funnels of an individual rising parcel of particles, respectively.

However, particle origins are <20 km upstream from the deployment location (the origin in the panels of Fig. 6). Faster sinking-particle funnels show complicated sampling patterns where horizontal and vertical variations in the sub-inertial current field create streaks from which sinking particles are collected.

The neutrally buoyant trap deployed at 300 m shows similar, though at times larger, displacement scales between the trap's location and the location of the collection and origin funnels (Fig. 7). This is especially striking considering the fact that the 300-m NBST was deployed a day less than the 500-m NBST (Table 2). Mean displacements of the 300-m NBST source funnels are 26 km distant from the trap for the 100-m/day sinking rate case and >35 km distant for the 50-m/day case (Table 2). Collection funnels are similar in character to those of the 500-m deployment (Fig. 6), though there are significant differences in the magnitude for

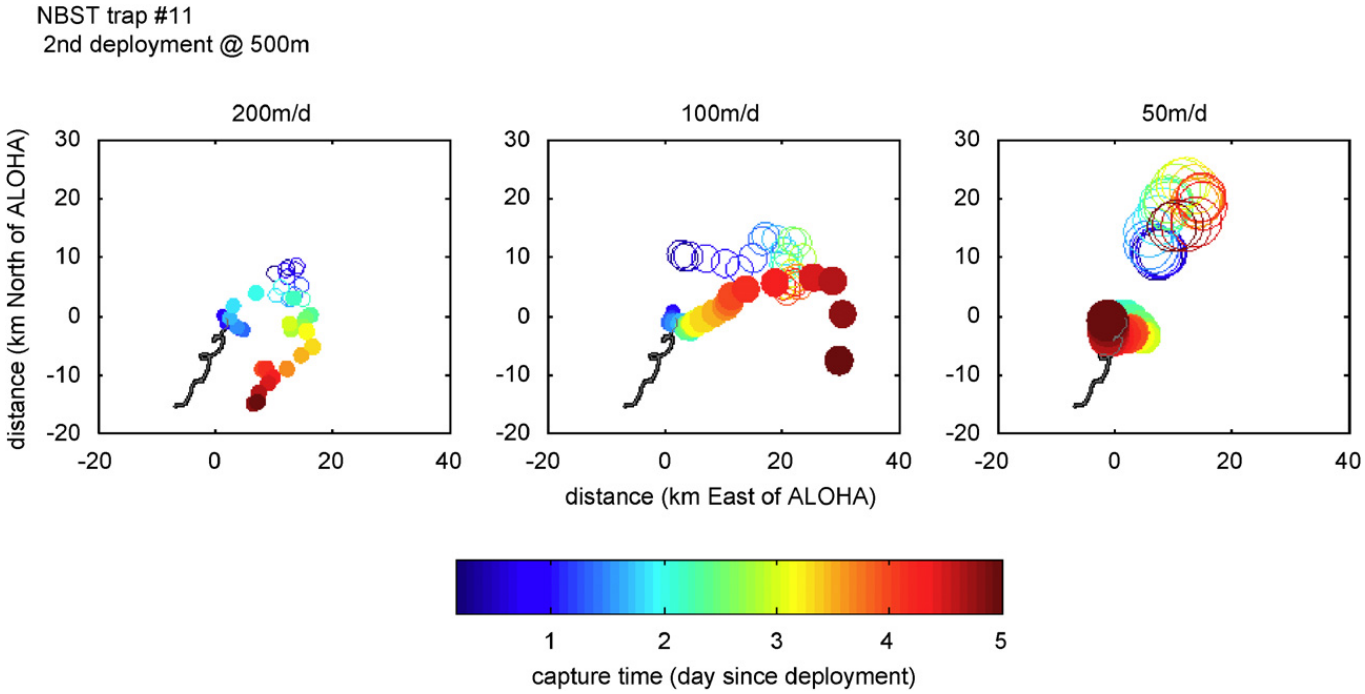

Fig. 6. Source (open circles) and collection (filled circles) funnels for NBST-11 (500-m depth) on its second deployment during VERTIGO-ALOHA for sinking speeds of 200 (left panel), 100 (middle panel) and 50 m/day (right panel). When source and collection funnels coincide they are plotted as filled circles. The color represents the age of the collection within the time course of the trap deployment. The deployment location is at the origin of each plot. The right panel ($S = 50$ m/day) is the same as the perspective diagram shown in Fig. 5.

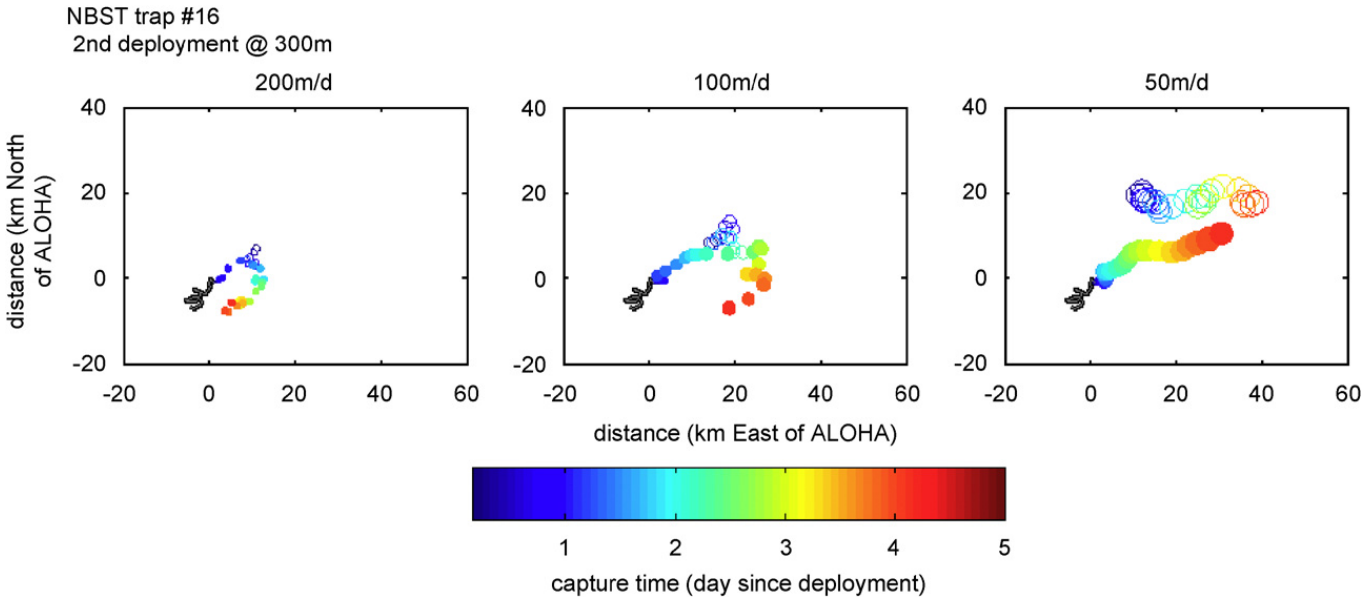

Fig. 7. Source (open circles) and collection (filled circles) funnels for NBST-16 (300-m depth) on its second deployment during VERTIGO-ALOHA for sinking speeds of 200 (left panel), 100 (middle panel) and 50 m/day (right panel). When source and collection funnels coincide they are plotted as filled circles. The color represents the age of the collection within the time course of the trap deployment. The deployment location is at the origin of each plot.

the 50-m/day case. Much of this is due to the greater effect of horizontal currents over the upper 150 m of the water column.

The 150-m neutrally buoyant trap travels considerably further than NBSTs deployed at the other depths (Table 1). It also travels north while the

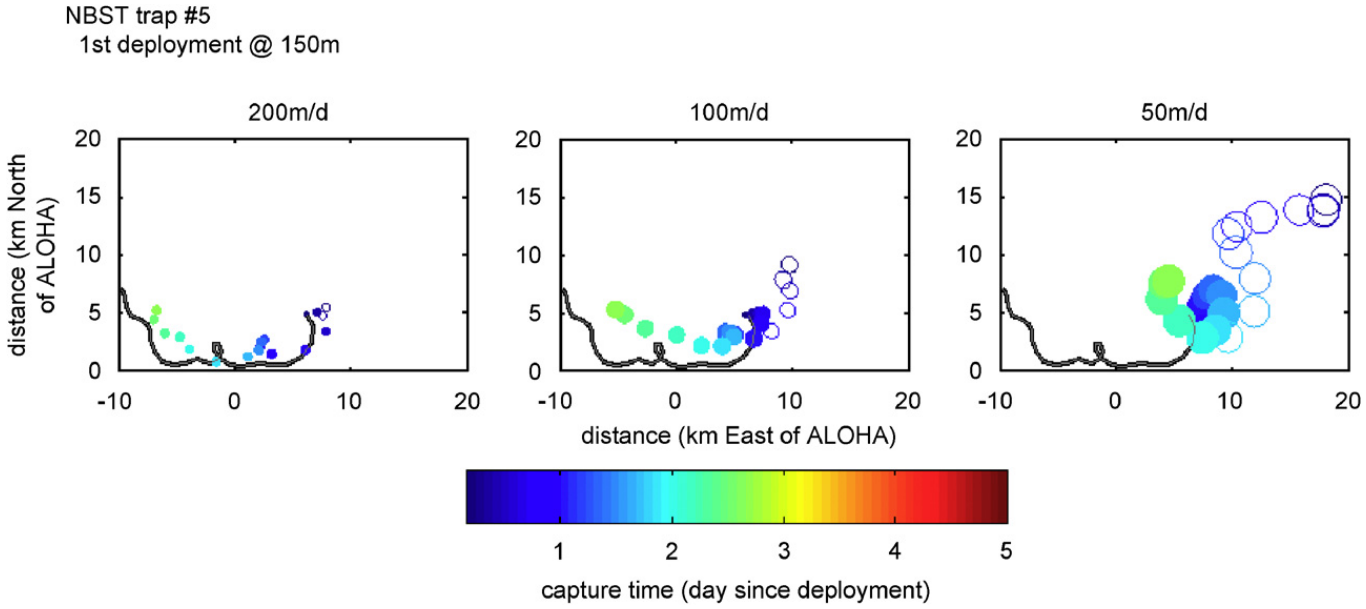

Fig. 8. Source (open circles) and collection (filled circles) funnels for NBST-13 (150-m depth) on its first deployment during VERTIGO-ALOHA for sinking speeds of 200 (left panel), 100 (middle panel) and 50 m/day (right panel). When source and collection funnels coincide they are plotted as filled circles. The color represents the age of the collection within the time course of the trap deployment. The deployment location is at the origin of each plot.

NBSTs at 300 and 500 m travel south. The source and collection funnels for the 150-m NBST during the first deployment are shown in Fig. 8. Source and collection funnels for the fast-sinking particles also overlap to a much greater extent than was observed at 500 m. The collection funnels generally follow the NBST, especially for the rapidly sinking particles. For the slowest sinking particles, the two funnel descriptions do not coincide and the source funnels are found upstream of trap location (Fig. 8).

Source and collection funnels for the three surface-tethered (clap) traps show a somewhat different pattern compared with those seen for the NBST deployments. Here, origin and collection funnels for the 150-, 300- and 500-m clap deployments are shown for deployment 2 for a sinking rate of 100 m per day (Fig. 9). For all three cases, the collection funnels are found mostly along the trap's trajectories, while the source funnels often diverge and are found mostly upstream of the trap's location. As expected, the source and collection funnels often overlap for the shallow-trap deployments while they mostly diverge for the deeper traps.

A synthesis of the spatial scales for the source and collection funnels of the drifting traps is provided in Table 2. Here, we determined the mean distance between the trap and the calculated collection and source funnels ($\bar{r}_c$ and $\bar{r}_s$), an estimate of spatial extent or patch scale of the individual collection and source funnels for a given deployment (r'_c and r'_s) and the size of an individual collection funnel (r^f_c and r^f_s). Also given in Table 2 is the mean depth from which the collected particles came during the trap's deployment (Z_c). For the 500-m NBST with a sinking rate of 50 m/day (Fig. 5), mean source-funnel displacements ($\bar{r}_s$) are 27 km from the trap's mean location, while the collection-funnel displacement is only ~8 km from the average location of the trap. For this deployment, the patch scale denoting the radial extent of collection funnels (r'_c) is 2.4 and 5.2 km for particle source funnels (r'_s). Last, the scales of each individual, instantaneous funnel, which are calculated using the residual currents, are quite small; values of r^f_c and r^f_s are 2.4 and 4.2 km, respectively.

Intuitively, the deeper the trap, the slower the sinking speed of the particle and the longer the collection period, the larger the floating trap sampling scales (Table 2). For a sinking rate of 100 m/day, mean source displacements ($\bar{r}_s$) vary from 4 to 26 km over the range of deployments, trap depths and drifting-trap types. The corresponding collection-funnel displacements ($\bar{r}_c$) are considerably less (2–18 km), as expected. Both mean displacements are larger for the second deployment than the first (Table 2). Surface-tethered mean trap source-funnel displacements are roughly one-half of those

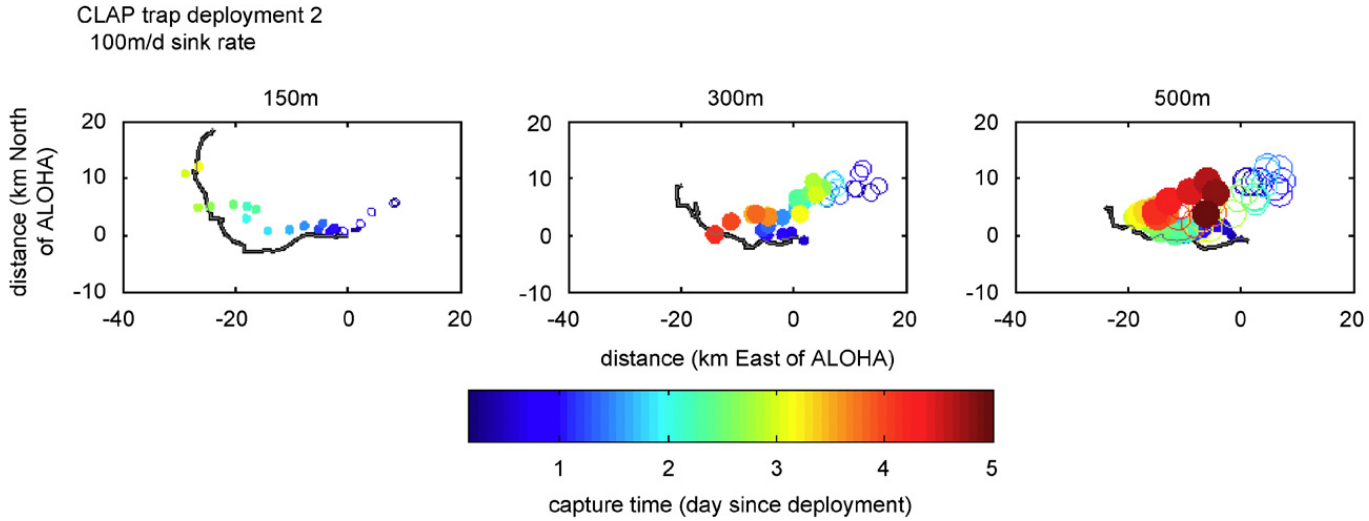

Fig. 9. Source (open circles) and collection (filled circles) funnels for the three clap traps from deployment 2 for a particle sinking rate of 100 m/day for clap traps deployed at 150 (left panel), 300 (middle panel) and 500 m (right panel). When source and collection funnels coincide they are plotted as filled circles. The color represents the age of the collection within the time course of the trap deployment. The deployment location is at the origin of each plot.

of the NBSTs. This is due to the fact that the neutrally buoyant traps are advected with the horizontal velocity at their deployment depth, while the surface-tethered traps are advected with a speed that is some vertical integration of the velocity profile above the trap. The sinking particles entering the trap will also be advected through the water column with a mean horizontal velocity more closely matched to the surface-tethered trap motions.

Statistical funnel patch scales are somewhat smaller than the displacement scales (Table 2). For a sinking rate of 100 m/day, source patch scales vary from 2 to 13 km while collection patch scales are 4–11 km in radial extent. As expected, there are no large differences in values of r'_c and r'_s between surface-tethered or neutrally buoyant trap deployments. The scales of each individual, instantaneous funnel (r^f_c and r^f_s) are rather small, 0.4–4.2 km depending on trap depth and deployment times. Values of r^f_s are larger than r^f_c due to the longer times over which source funnels are calculated for deep traps and slow sinking speeds.

Finally, estimates of the rate at which the displacement and patch source funnels grow in time ($\Delta\bar{r}_s/\Delta t$ and $\Delta r'_s/\Delta t$) can be made by dividing these scales by the deployment duration (Table 2). For the neutrally buoyant trap at 500 m, the displacement source-funnel scale will grow at a rate of ~5 km/day for sinking rates of 50 and 100 m/day and at 3 km/day for the 200-m/day case. Patch source-funnel scales grow slower at rates of 1–1.7 km/day. Source-funnel mean displacement scales grow faster for the neutrally buoyant traps and for the second deployment (Table 2).

The superposition of source funnels from different trap types and deployment depths for the second deployment is shown in Fig. 10. All source funnels are found within a ~50 km sized window centered at the deployment location (the origin in Fig. 10). The extent of the particle source regions shrinks as the particle sinking rate increases, but not as dramatically as one might expect. As expected, the shallower the trap and the faster the sinking rate, the narrower the "sampling stripe" at the sea surface. However, the lengths of the stripes are roughly similar for all depths and sinking rates. The type of trap (neutrally buoyant vs. surface tethered) has little bearing on the basic pattern of the sampling stripe, although the locations of the stripes often diverge.

Importantly, the particle source funnels do not coincide for different traps, deployment depths or particle sinking rates (Fig. 10). Trap material collected at 500 m may have come from as far as 50 km distance from that collected by the trap at 150-m depth. This result is roughly independent of either trap type or mean particle sinking speed. Further, trap material of different sinking speeds collected in a single trap can have distant source locations. For example, the NBST trap at 500 m collects 50-m/day sinking particles with source locations that are ~27 km to the NNE, while it collects 200-m/day sinking particles ~15 km distant but now from the ESE (Table 2).

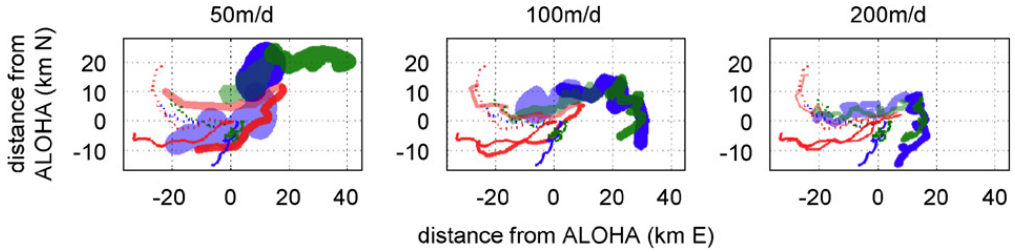

Fig. 10. Source funnels for NBST and clap traps during the second deployment for 50, 100 and 200 m/day in the left, middle and right panels, respectively. Each basic color represents a different deployment depth: blue: 500 m, green: 300 m and red: 150 m. The darker for each of the primary colors shows the NBST funnels and the solid lines represent the paths of the NBST. The lighter colored funnels and dashed lines represent clap trap funnels and locations, respectively. For clarity, corresponding collection funnels are not shown.

6. Source-funnel scales for a deep-moored trap

The assessment of source funnels for fixed moored traps requires the integration of the horizontal advection over much longer time and space scales requiring the use of geostrophic currents derived from the satellite altimeter absolute sea level distributions (Fig. 1). To project the surface currents to depth, we created a mean sub-inertial speed profile from all available ADCP data from cruises to Station ALOHA aboard the R/V *Kilo Moana* during 2004 (Fig. 11). Beyond the range of the ADCP (1200 m), a constant value was assumed extending this profile to 4000 m. The effects of vertical current shear are most important over the upper 300 m of the water column (Fig. 11).

Deep-trap source-funnel scales are calculated by advecting particles backward in time as they rise using the satellite altimetry surface currents and the sub-inertial speed profile. Calculations are made for the deep-moored trap at 4000 m from November 10, 2001, to November 6, 2004, for particle sinking rates of 50, 100 and 200 m/day. Individual particles are released daily, and their back trajectories are estimated with a time step of 6 h. Other schemes for propagating the surface currents to depth resulted in quantitatively similar results.

The calculated source locations (Fig. 12) show complicated patterns of deep-sea sediment trapping as first discussed by Siegel and Deuser (1997). Containment radii ($R_{95\%}$), defined as the radial distance containing 95% of the source origins, are 126, 215 and 339 km for mean particle sinking speeds of 200, 100 and 50 m/day, respectively. Mean displacement distances are all to the north–northeast for distances of 17, 28 and 54 km again for sinking rates of 200, 100 and 50 m/day, respectively.

The spaghetti diagram of source locations shown in Fig. 12 illustrates the ephemeral nature of the sampling by moored deep-sea traps. Each dot in Fig. 12 is a daily estimate of the source region. The spread of each release due to residual currents is estimated to be ~10 km (Siegel and Deuser, 1997).

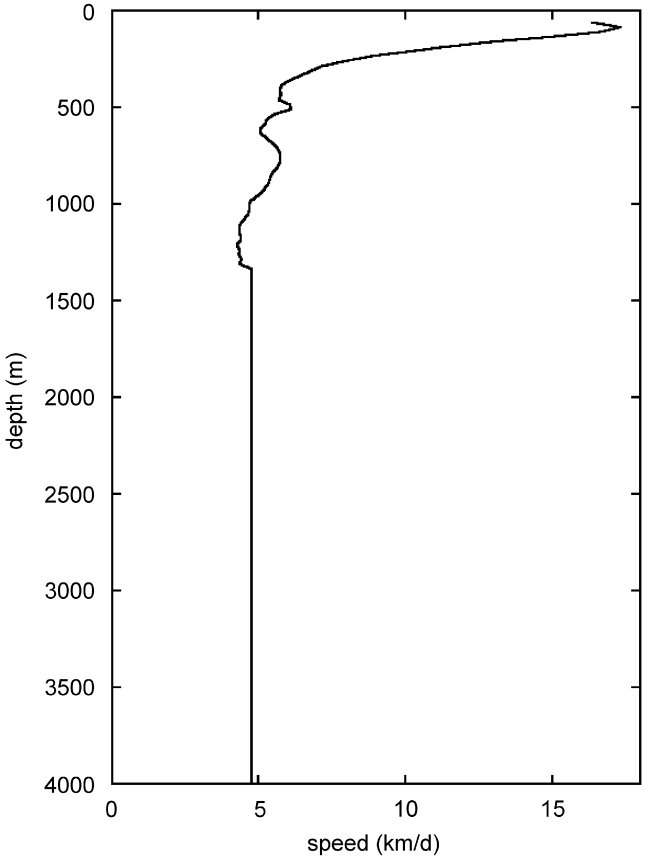

Fig. 11. Sub-inertial time scale root-mean-squared (RMS) horizontal current profile used in extrapolating altimetric surface current estimates to depth. ADCP data from all cruises of the R/V *Kilo Moana* for 2004 were used for all multiday occupations of Station ALOHA when the narrow band ADCP system was available. Horizontal velocity estimates from the narrowband ADCP were filtered to remove tidal and diurnal scale currents and are then used to estimate RMS current profile. Below 1400 m, a constant RMS current speed is assumed.

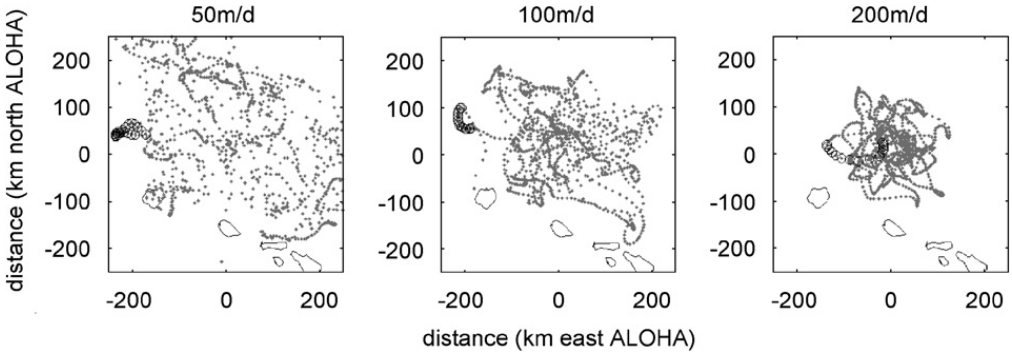

Fig. 12. Source locations for collected particles by the HOT moored sediment trap at 4000 m for 3 years (November 10, 2001–November 6, 2004) for sinking speeds of 50 (left), 100 (center) and 200 m/day (right panel). Each dot is the source location for a particle collected each day for the 3 years of data where the origin is placed at Station ALOHA. The open circles represent source-funnel locations for the respective sinking rate during VERTIGO (June 25–July 10, 2004).

A 20-day cup collection will integrate along 20 of these individual source locations, which can stretch from many 10s of km to several 100 km (Fig. 12).

Particle source funnels for the period June 25–July 10, 2004, are shown as the open circles in Fig. 12. For the two slower sinking speeds modeled, the source funnels are >200 km east of Station ALOHA (Table 4). However, for the 200-m/day sinking particles, the source regions are much closer to Station ALOHA at a mean distance 73 km. Clearly, a trap collection of a mixture of sinking rates will have a corresponding mixture of particle source origins.

7. Discussion

The sampling characteristics of near-surface drifting, neutrally buoyant and deep-sea moored sediment traps show many similarities as well as many important differences. We show a general correspondence of sampling scales for the upper-ocean traps and large differences when compared with deep-moored traps. When viewed in detail, source and collection funnels for upper-ocean traps show significant differences at submesoscales (<60 km). The importance of these differences will depend on the spatial distribution of particle export. If export is spatially uniform, these differences will be irrelevant. However, if there are spatial gradients in the magnitude of flux or composition of particles, knowledge of the source and collection funnels will be important. In the following, we discuss the differences in collection scales between the deep- and upper-ocean sediment traps, assess whether differences in source-funnel distributions matter for the interpretation of VERTIGO sinking flux experiments and present some implications resulting from our modeling of trap sampling characteristics.

7.1. Funnel scales for deep-ocean moored vs. upper-ocean drifting traps

The sampling characteristics of near-surface drifting and deep-sea moored traps have very different patterns. A deep-moored trap samples export from a streak at the upper ocean that is many 10s to ~100 km long and about 10 km wide, and these streaks can be offset several 100 km from the trap (Fig. 12). For the deep-moored trap presented here, 95% containment radii range from 126 to nearly 350 km for mean sinking rates from 200 to 50 m/day. On the other hand, drifting upper-ocean traps sample much smaller scales both in their spatial extent and mean displacement from the trap (both are typically less than 25 km; Fig. 10). These smaller sampling scales are driven by the shorter sinking times and collection intervals for upper-ocean trap deployments, as well as the fact that the traps are embedded in the flow field.

Clearly, it takes longer for a particle to sink into a deep-moored trap than a shallow one. This difference has a dominant role in determining source-funnel characteristics. A particle sinking at 100 m/day will be sampled by a trap at 300 m in 3 days but will take 40 days to reach a trap at 4000 m. For upper-ocean traps, estimates of the growth rate for a source-funnel patch and displacement scales are roughly 1–2 km per day (Table 2). Extrapolating these results to 40 days, the patch and displacement scales could be as much as 100 km. This is likely a large overestimate as deep-ocean current speeds are much smaller than those in the upper 300 m

(Fig. 11). Considering that the sub-inertial currents averaged over the entire water column are roughly a factor of 2 smaller than RMS values just for the upper 300 m, the extrapolation of the upper-ocean trap patch and displacement growth scales to the deep ocean will be roughly 50 km. This estimate is considerably smaller than the observed source-funnel scales for the deep traps (Fig. 12; Table 4). The relative advection of the falling rain of particles will be influenced by only a subset of the scales of motion for a drifting trap while a trap that is fixed in space will be affected by all scales of motion. Thus, the sampling scale for a moored deep-ocean trap will be larger than the drifting-trap result extrapolated to longer sinking times.

7.2. Do particle source funnels matter?

The present analyses describe the sampling of the rain of sinking particles as a function of trap type, deployment depth and particle sinking rate. The superposition of source funnels shown in Fig. 10 demonstrates that upper-ocean traps deployed at different depths sample somewhat different oceans. Distances between source funnels for the same deployment can be as much as 20 km, depending on trap depth and particle sinking rate. The collection of source funnels, such as shown in Fig. 10, provides a reasonable way for bounding the regional scale over which an upper-ocean sediment-trap experiment is conducted. A cursory examination of Fig. 10 shows this regional scale for upper-ocean trap collection is something smaller than 60 km. For a deep-ocean moored trap, the regional bounding scales are much larger and can be more than 300 km (Fig. 12).

The assessment of the importance of trap sampling characteristics requires synoptic maps of particle export. Observations of this type are obtainable only through the application of a model of particle export to large-scale determinations of productivity or phytoplankton biomass such as those available from satellite ocean color data sets (e.g., McClain et al., 2004a; Behrenfeld et al., 2006). Here, we use satellite determinations of upper layer chlorophyll concentration as a proxy for the spatial distribution of particle export. Multi-mission merged satellite imagery is used to increase the availability of good data because of cloudiness (see http://oceancolor.gsfc.nasa.gov/forum/oceancolor/topic_show.pl?tid=1141 for details). Chlorophyll data from MODIS/Aqua and SeaWiFS are merged daily at a resolution of 9 km and then averaged over the period June 25–July 10, 2004.

Over large scales (~1000 km), chlorophyll concentrations vary by roughly a factor of 5 (Fig. 13a). However, within 60 km of Station ALOHA (Fig. 13b), these changes are much smaller. In the vicinity of Station ALOHA, values of chlorophyll range from 0.05 to 0.13 mg/m^3 (Fig. 13b) and are typical of the North Pacific Subtropical Gyre (McClain et al., 2004b). Higher values of chlorophyll ($>0.15\,mg/m^3$) are found 200–600 km to the WNW of Station ALOHA (which is at the center of the red box in Fig. 13a). These regions of elevated chlorophyll concentration are similar in spatial extent to the open-ocean phytoplankton blooms discussed by Wilson (2003) although these observations are considerably smaller in magnitude.

Estimates of mean chlorophyll concentration for each of the upper-ocean trap source funnels from Fig. 10 and from Station ALOHA and a 60 km box surrounding Station ALOHA are given in Table 3. Source-funnel chlorophyll values range from 0.064 to 0.075 mg/m^3 (Table 3). They are smaller for the slower sinking particles and deeper traps and are higher for shallow traps and rapidly sinking particles. However, these chlorophyll differences are quite small relative to Station ALOHA and range from −4.7% to 10.5% and average 3.5% higher. The differences in chlorophyll between the source-funnel locations for the 150–500-m traps and Station ALOHA range over 15%. However, differences in flux attenuation are much larger, as POC flux decreases by 80% between 150 and 500 m (Buesseler et al., 2007a). Thus, this range in chlorophyll between funnels is fairly small when attenuation of flux vs. depth is considered, and will have little bearing on the interpretation of flux measurements during VERTIGO.

This same exercise can be repeated for the deep traps (Table 4). Much larger differences in chlorophyll are found between observations at Station ALOHA, the 95% containment radii enclosure and the estimated source locations for VERTIGO experiment. Percentage differences in the chlorophyll concentrations between Station ALOHA and averaged over the containment radii are 20.4–26.5%, where the smallest differences occur for the 200-m/day sinking rate (Table 4). In contrast are the small differences observed during the VERTIGO cruises, where the percent differences between the deep-trap source-funnel locations (Fig. 12) and chlorophyll at Station ALOHA are less than 5% (Table 4).

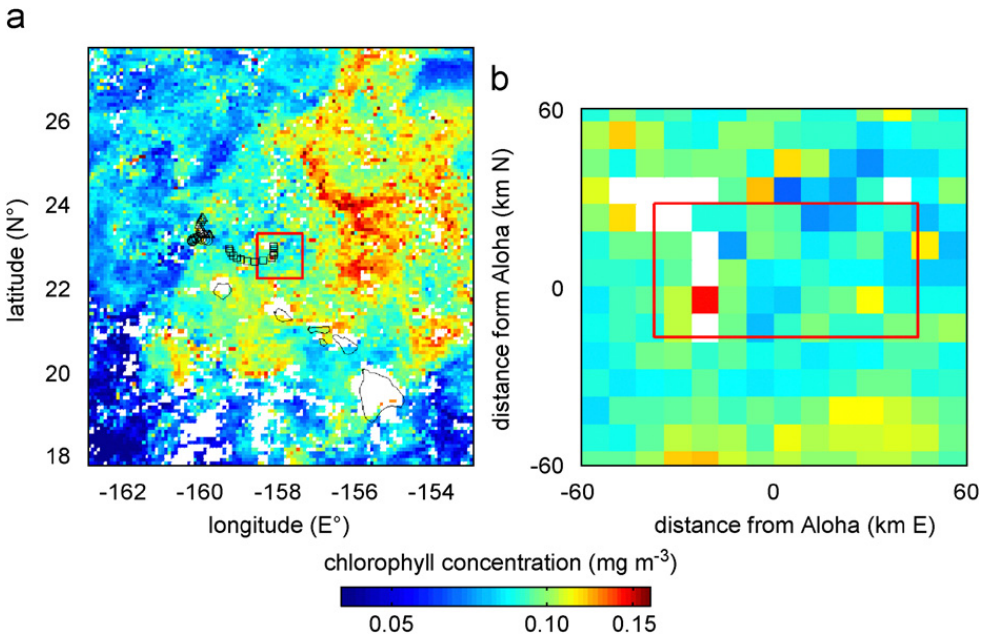

Fig. 13. Satellite chlorophyll concentration distribution for the period June 25–July 10, 2004, for (a, left panel) the region north of the Hawaiian Islands and (b, right panel) a 120 km × 120 km square region focused on the VERTIGO experiment. The location of the high-spatial-resolution image of the right panel image is shown as the red square in the left image and the red square in the right panels represents the domain of Fig. 10. Chlorophyll data from MODIS/Aqua and SeaWiFS are merged to two 8-day composites at a resolution of 9 km which are averaged to provide imagery for the period June 25–July 10, 2004. Details of the merging method can be found at http://oceancolor.gsfc.nasa.gov/forum/oceancolor/topic_show.pl?tid=1141. Locations of daily source regions for the moored traps at 4000 m (from Fig. 12) are shown in the left panel for sinking rates of 50 (circles), 100 (triangles) and 200 m per day (squares).

Table 3
Chlorophyll values for the shallow-trap source funnels during deployment 2 of VERTIGO-ALOHA

Trap type	Trap depth (m)	Sinking rate (m/day)	Mean chl. (mg/m^3)	Stan. dev. chl. (mg/m^3)	# Pixels (–)	Differences from ALOHA (%)
Station ALOHA			0.0642	0.0017	9	–
60 km box at Station ALOHA			0.0728	0.0118	44	7.5
NBST	150	050	0.0680	0.0026	120	0.4
NBST	300	050	0.0657	0.0035	217	−3.0
NBST	500	050	0.0645	0.0037	247	−4.7
NBST	150	100	0.0718	0.0088	65	6.1
NBST	300	100	0.0734	0.0077	133	8.4
NBST	500	100	0.0708	0.0057	271	4.6
NBST	150	200	0.0747	0.0115	33	10.3
NBST	300	200	0.0713	0.0027	47	5.3
NBST	500	200	0.0718	0.0030	120	6.1
Clap	150	050	0.0696	0.0044	124	2.8
Clap	300	050	0.0665	0.0026	170	−1.8
Clap	500	050	0.0695	0.0064	482	2.7
Clap	150	100	0.0729	0.0064	68	7.7
Clap	300	100	0.0673	0.0024	135	−0.6
Clap	500	100	0.0668	0.0021	213	−1.3
Clap	150	200	0.0747	0.0084	40	10.3
Clap	300	200	0.0714	0.0080	74	5.5
Clap	500	200	0.0704	0.0082	149	4

This high degree of correspondence between chlorophyll concentration at Station ALOHA and the modeled deep-trap source regions during the VERTIGO sampling is mostly fortuitous. The present exercise can be repeated for each of the daily source regions for the 3-year time series

Table 4
Chlorophyll values for the deep-trap funnels during VERTIGO-ALOHA

	Sinking rate (m/day)	Radial distance (km)	Mean chl. (mg/m^3)	Stan. dev. chl. (mg/m^3)	# Pixels (–)	Differences from ALOHA (%)
Station ALOHA	–	–	0.0642	0.0017	9	–
120 km box	–	–	0.0736	0.0102	158	14.8
$r < R_{95\%}$	50	339	0.0812	0.0230	4253	26.5
$r < R_{95\%}$	100	215	0.0815	0.0156	1715	27.1
$r < R_{95\%}$	200	126	0.0772	0.0116	605	20.4
6/25/2004–7/10/2004	50	226	0.0656	0.0001	16	2.2
6/25/2004–7/10/2004	100	216	0.0656	0.0001	15	2.2
6/25/2004–7/10/2004	200	73	0.0668	0.0003	15	4.1

modeled in Fig. 12 using available satellite chlorophyll data. Normalized RMS differences for chlorophyll concentration between all of the modeled source locations and Station ALOHA range from 20% to 24% depending on sinking rate. The percentage differences in chlorophyll between source locations and Station ALOHA exceed 25% for 14–29% of the time during the 3-year record (for sinking rates ranging from 50 to 200 m/day). Hence, interpretations of deep-trap fluxes from Station ALOHA should consider the effects of spatial inhomogeneities in particle source locations. Comparisons of the upper-ocean traps to the deep-moored trap will also be confounded by this issue, since in this case during VERTIGO the deep trap will be sampling a potentially higher particle source region than the shallow traps. It is easy to envision how one could misinterpret the rates of remineralization for sinking particles if particle source funnels are not considered.

Clearly, the oligotrophic Pacific is not where one expects to find large gradients in particle export, and one would expect much larger spatial and temporal changes in particle flux at other locations (e.g., Lampitt and Antia, 1997). We find that for Station ALHOA an understanding of source funnels is important for the interpretation of deep-sea sediment flux determinations and for making connections between shallow and deep flux estimates. However, for shallow traps, this understanding is not critical—at least for the conditions assessed here.

Last, the use of surface-layer chlorophyll concentrations as a proxy for the distribution of particle export may underestimate the importance of source funnels. If the spatial distributions of chlorophyll and export are similar, then the use of chlorophyll as a proxy for export is reasonable. However, power spectra for phytoplankton have redder wavenumber spectra than do zooplankton (e.g., Mackas and Boyd, 1979; Abraham, 1998). This means that more of the variance in phytoplankton concentrations (as inferred from chlorophyll) is contained on larger scales than for zooplankton abundances. The key here is whether export is controlled by phytoplankton (via primary productivity) or by zooplankton (via grazing). If grazing dominates export, spatial variability in export will be on scales much smaller than chlorophyll and the present analysis maybe a best case scenario. The resolution of this issue is beyond the scope of this paper though it has an important bearing on the importance of statistical funnels on the assessment of export.

7.3. Implications for studying the ocean's biological pump

This study demonstrates the scales of source and collection funnels and the importance of knowing trap sampling characteristics in the interpretation of export-flux experimental results. The assessment of the vertical rain of sinking particles is limited by (1) the traps themselves, (2) our inability to continuously sample upper-ocean particle fluxes and (3) the sampling of a spatially heterogeneous rain of particles from single points in space. Here, our focus has been on how sediment traps sample the spatially complex and temporally episodic particle rain and the degree to which these limitations influence the interpretation of trap data sets.

Our work provides insights on how one might best assess the heterogeneous particle flux experimentally using a coordinated campaign of sediment trapping, horizontal current mapping, remote sensing, numerical modeling and retrospective data analyses. This interpretive support will allow the

role of time/space variability of export around sediment traps to be assessed. Satellite ocean color imagery can be used to determine the time/space variability of chlorophyll and net primary production surrounding each deployment, enabling us to assess the importance of episodic blooms and their importance for particular source funnels. Satellite altimetric estimates of sea level and geostrophic velocity as well as satellite vector winds can be used to drive data assimilation models of the time-dependent circulation (e.g., McGillicuddy and Kosnyrev, 2001). This will provide the velocity data required to estimate particle source funnels and will enable one to assess the relationships between measured trap fluxes vs. depth while sampling a possibly heterogeneous export field. Thus, it seems that progress in understanding production–export relationships will require the simultaneous determination of the particle source funnels as well as the spatial and temporal fields of particle export and the vertical profile of sinking-particle flux using sediment traps.

Acknowledgments

We gratefully acknowledge the National Science Foundation's Chemical and Biological Oceanography Programs (Grants OCE-0327318 and OCE-03-01139) and the Department of Energy's Carbon Sequestration Program (Grant DE-FG02-03ER63697) for supporting our work on VERTIGO. Detailed comments and suggestions from the editors Richard Matear and Mike Bacon as well as by the anonymous reviewers greatly improved the presentation of this work. Jules Hummon helped with the acquiring and processing of the ADCP data from the R/V *Kilo Moana*. Altimeter products were produced by Ssalto/Duacs and distributed by AVISO with support from CNES. Merged ocean color imagery is courtesy of the NASA Ocean Color Data Processing Group at the Goddard Space Flight Center.

References

Abraham, E.R., 1998. The generation of plankton patchiness by turbulent stirring. Nature 391, 577–580.

Armstrong, R.A., Lee, C., Hedges, J.I., Honjo, S., Wakeham, S.G., 2002. A new, mechanistic model for organic carbon fluxes in the ocean based on the quantitative association of POC with ballast minerals. Deep-Sea Research II 49, 219–236.

Asper, V.L., 1996. Particle flux in the ocean: oceanographic tools. In: Ittekloft, V., Schäfer, P., Honjo, S., Depetris, P.J. (Eds.), Particle Flux in the Ocean. Wiley, Chichester, UK, pp. 71–81.

Asper, V.L., Deuser, W.G., Knauer, G.A., Lohrenz, S.E., 1992. Rapid coupling of sinking particle fluxes between surface and deep ocean waters. Nature 357, 670–672.

Behrenfeld, M.J., O'Malley, R.T., Siegel, D.A., McClain, C.R., Sarmiento, J.L., Feldman, G.C., Milligan, A.J., Falkowski, P.G., Letelier, R.M., Boss, E.S., 2006. Climate-driven trends in contemporary ocean productivity. Nature 444, 752–755.

Berelson, W.M., 2002. Particle settling rates increase with depth in the ocean. Deep-Sea Research II 49, 237–251.

Bretherton, F.P., Davis, R.E., Fandry, C.B., 1976. A technique for objective analysis and design of oceanographic experiments applied to MODE-73. Deep-Sea Research 23, 559–582.

Buesseler, K.O., 1992. Do upper-ocean sediment traps provide an accurate record of particle flux? Nature 353, 420–423.

Buesseler, K.O., 1998. The decoupling of production and particulate export in the surface ocean. Global Biogeochemical Cycles 12, 297–310.

Buesseler, K.O., Michaels, A.F., Siegel, D.A., Knap, A.H., 1994. A three dimensional time-dependent approach to calibrating sediment trap fluxes. Global Biogeochemical Cycles 8, 179–193.

Buesseler, K.O., Steinberg, D.K., Michaels, A.F., Johnson, R.J., Andrews, J.E., Valdes, J.R., Price, J.F., 2000. A comparison of the quantity and composition of material caught in a neutrally buoyant versus surface-tethered sediment trap. Deep-Sea Research I 47, 277–294.

Buesseler, K.O., Lamborg, C.H., Boyd, P.W., Lam, P.J., Trull, T.W., Bidigare, R.R., Bishop, J.K.B., Casciotti, K.L., Dehairs, F., Elskens, M., Honda, M., Karl, D.M., Siegel, D.A., Silver, M.W., Steinberg, D.K., Valdes, J., Van Mooy, B., Wilson, S., 2007a. Revisiting carbon flux through the ocean's twilight zone. Science 316, 567–570.

Buesseler, K.O., Antia, A.N., Chen, M., Fowler, S.W., Gardner, W.D., Gustaffson, Ö., Harada, K., Michaels, A.F., Rutgers van der Loeff, M., Sarin, M., Steinberg, D.K., Trull, T., 2007b. An assessment of the use of sediment traps for estimating upper ocean particle fluxes. Journal of Marine Research 65 (3), 345–416.

Christian, J.R., Lewis, M.R., Karl, D.M., 1997. Vertical fluxes of carbon, nitrogen, and phosphorous in the North Pacific Subtropical Gyre near Hawaii. Journal of Geophysical Research 102, 15667–15677.

Coale, K.H., 1990. Labyrinth of doom: a device to minimize the "swimmer" component on sediment trap collections. Limnology and Oceanography 35, 1376–1380.

Daley, R., 1994. Atmospheric Data Analysis. Cambridge University Press, Cambridge, 471pp.

Deuser, W.G., Müller-Karger, F.E., Evans, R.H., Brown, O.B., Esaias, W.E., Feldman, G.C., 1990. Surface-ocean color and deep-ocean carbon flux: how close a connection? Deep-Sea Research I 37, 1331–1343.

de Haan, P., Rotach, M.W., 1998. A novel approach to atmospheric dispersion modelling: the puff-particle model. Quarterly Journal of the Royal Meteorological Society 124, 2771–2792.

Fasham, M.J.R. (Ed.), 2003. Ocean Biogeochemistry: the Role of the Ocean Carbon Cycle in Global Change. Springer, Berlin, 297pp.

Firing, E., 1996. Currents observed north of Oahu during the first 5 years of HOT. Deep-Sea Research II 43, 281–303.

Gardner, W.D., 2000. Sediment trap sampling in surface waters. In: Hanson, R.B., Ducklow, H.W., Field, J.G. (Eds.), The Changing Ocean Carbon Cycle, a Midterm Synthesis of the Joint Global Ocean Flux study. International Geosphere–Biosphere Programme Books Series, vol. 5. Cambridge University Press, Cambridge, pp. 240–281.

Gust, G., Michaels, A.F., Johnson, R., Deuser, W.G., Bowles, W., 1994. Mooring line motions and sediment trap hydrodynamics: in situ intercomparison of three common deployment designs. Deep-Sea Research I 41, 831–857.

Hansell, D.A., Newton, J.A., 1994. Design and evaluation of a "swimmer"-segregating particle interceptor trap. Limnology and Oceanography 39, 1487–1495.

Karl, D.M., Knauer, G.A., 1989. Swimmers: a recapitulation of the problem and a potential solution. Oceanography 2, 32–35.

Karl, D.M., Christian, J.R., Dore, J.E., Hebel, D.V., Letelier, R.M., Tupas, L.M., Winn, C.D., 1996. Seasonal and interannual variability in primary production and particle flux at Station ALOHA. Deep-Sea Research II 43, 539–568.

Lampitt, R.S., Antia, A.N., 1997. Particle flux in deep seas: regional characteristics and temporal variability. Deep-Sea Research I 44, 1377–1403.

Lampitt, R.S., Sanders, R.J., Boorman, B., Brown, L., Guyard, P.H., Leaute, F.J., Popova, E.E., Saw, K.A., Turnewitsch, R., Zubkov, M.V., 2004. Particulate export in the northeast Atlantic: an integrated attack using production rates, tracers and a novel drifting sediment trap. In: ASLO/TOS Ocean Research Conference, Honolulu, HI, p. 87.

Leben, R.R., Born, G.H., Engebreth, B.R., 2002. Operational altimeter data processing for mesoscale monitoring. Marine Geodesy 25, 3–18.

Mackas, D.L., Boyd, C.M., 1979. Spectral analysis of zooplankton spatial heterogeneity. Science 204, 62–64.

Martin, J.H., Knauer, G.A., Karl, D.M., Broenkow, W.W., 1987. VERTEX: carbon cycling in the northeast Pacific. Deep-Sea Research Part A. Oceanographic Research Papers 34, 267–285.

Maury, M.F., 1858. The Physical Geography of the Sea. Harper & Brothers, New York.

McClain, C.R., Feldman, G.C., Hooker, S.B., 2004a. An overview of the SeaWiFS project and strategies for producing a climate research quality global ocean bio-optical time series. Deep-Sea Research II 51, 5–42.

McClain, C.R., Signorini, S.R., Christian, J.R., 2004b. Subtropical gyre variability observed by ocean color satellites. Deep-Sea Research II 51, 281–301.

McGillicuddy, D.J., Kosnyrev, V.K., 2001. Dynamical interpolation of mesoscale flows in the TOPEX/Poseidon diamond surrounding the US JGOFS Bermuda Atlantic time-series site. Journal of Geophysical Research 106, 16641–16656.

McGillicuddy Jr., D.J., Robinson, A.R., Siegel, D.A., Jannasch, H.W., Johnson, R., Dickey, T.D., McNeil, J., Michaels, A.F., Knap, A.H., 1998. Influence of mesoscale eddies on new production in the Sargasso Sea. Nature 394, 263–265.

Michaels, A.F., Knap, A.H., 1996. Overview of the US JGOFS Bermuda Atlantic Time-Series Study and the Hydrostation S Program. Deep-Sea Research II 43, 157–198.

Michaels, A.F., Silver, M.W., Gowing, M.M., Knauer, G.A., 1990. Cryptic zooplankton "swimmers" in upper ocean sediment traps. Deep-Sea Research 37, 1285–1296.

Peterson, M.L., Hernes, P.J., Thoreson, D.S., Hedges, J.I., Lee, C., Wakeham, S.G., 1993. Field evaluation of a valved sediment trap designed to minimize collection of swimming animals. Limnology and Oceanography 38, 1741–1761.

Siegel, D.A., Deuser, W.G., 1997. Trajectories of sinking particles in the Sargasso Sea: modeling of statistical funnels above deep-ocean sediment traps. Deep-Sea Research I 44, 1519–1541.

Siegel, D.A., Granata, T.C., Michaels, A.F., Dickey, T.D., 1990. Mesoscale eddy diffusion, particle sinking and the interpretation of sediment trap data. Journal of Geophysical Research 95, 5305–5311.

Siegel, D.A., McGillicuddy Jr., D.J., Fields, E.A., 1999. Mesoscale eddies, satellite altimetry and new production in the Sargasso Sea. Journal of Geophysical Research 104, 13359–13379.

Stanley, R.H.R., Buesseler, K.O., Manganini, S.J., Steinberg, D.K., Valdes, J.R., 2004. A comparison of major and minor elemental fluxes collected using neutrally buoyant and surface-tethered traps. Deep-Sea Research I 51, 1387–1395.

Valdes, J.R., Price, J.F., 2000. A neutrally buoyant, upper ocean sediment trap. Journal of Atmospheric and Oceanographic Technology 17, 62–68.

Waniek, J., Koeve, W., Prien, R.D., 2000. Trajectories of sinking particles and the catchment areas in the North East Atlantic. Journal of Marine Research 58, 983–1006.

Waniek, J.J., Schulz-Bull, D.E., Blanz, T., Prien, R.D., Oschlies, A., Müller, T.J., 2005. Interannual variability of deep water particle flux in relation to production and lateral sources in the northeast Atlantic. Deep-Sea Research I 52, 33–50.

Wilson, C., 2003. Late summer chlorophyll blooms in the oligotrophic North Pacific Subtropical Gyre. Geophysical Research Letters 30.